

SUPPORTING INFORMATION

Photocatalytic Decarboxylation of Lactic acid by Pt/TiO₂

Kaituo Liu,^[a] Anton Litke,^[a] Yaqiong Su,^[a] Bart G. van Campenhout,^[a] Evgeny A. Pidko,^{*, [a,b]} Emiel
J.M. Hensen^{*,[a]}

^a Inorganic Materials Chemistry group, Schuit Institute of Catalysis and ^b Institute for Complex Molecular Systems, Eindhoven University of Technology, P.O. Box 513, 5600 MB Eindhoven, The Netherlands.

Corresponding authors: Evgeny A. Pidko (e.a.pidko@tue.nl)
Emiel J.M. Hensen (e.j.m.hensen@tue.nl)

Contents

S1. Experimental and Computational details	3
S1.1. Catalyst preparation	3
S1.2. Physical chemical characterization	3
S1.3. Photolysis and photocatalysis activity tests	4
S1.4. Periodic DFT calculations	5
S1.5. Time-dependent DFT calculations	6
S2. Supplementary computational and experimental results	6
S2.1. Photolysis of aqueous lactic acid	6
S2.2. Time-dependent DFT calculations	8
S2.3. Supplementary results of 2D NMR analysis and photoelectrochemical tests	12
S2.4. Photocatalytic conversion of ethanol and pyruvic acid	14
S2.5. Lactic acid adsorption on TiO₂ surface	15
S2.6. Periodic DFT calculations on lactic acid decarboxylation over Pt₁₀/TiO₂ model	16
S2.7. TD-DFT calculations on a TiO₂-bound surface lactate model	18
S2.8. Acceptorless Dehydrogenative Coupling of lactic acid	20
S3. References	22

S1. Experimental and Computational details

S1.1. Catalyst preparation

In most experiments commercial nanocrystalline TiO₂ (Aeroxide P25) was used. The noble metal loading in all samples was 1.0 wt. %. The Au/TiO₂ photocatalyst was prepared by a deposition-precipitation method involving urea as described previously¹. A 100 mL solution containing HAuCl₄ (1 mM), 0.6 g urea and 1.98 g TiO₂ were mixed and stirred at 80 °C for 4 h in darkness. The resulting solid was washed with deionised water, dried under vacuum at room temperature for 12 h and then reduced in a tubular oven in H₂ flow at 300 °C for 4h. Other noble metal (Pt, Pd, and Ru) containing TiO₂ photocatalysts were prepared by impregnation followed by reduction. An amount of 1 g of P25 TiO₂ powder was impregnated with 27 mL aqueous solutions of H₂PtCl₆, PdCl₂, or RuCl₃ at a metal concentration of 0.37 mg/mL. This suspension was stirred for 3 h at room temperature. The suspension was then evaporated in a water bath at 80°C followed by drying in an oven at 110°C overnight. The resulting powders were ground and reduced in a tubular oven in H₂ flow at 300 °C for 4 h. Two further Pt/TiO₂ samples were prepared in the same way starting from anatase and rutile forms of TiO₂ (Sigma Aldrich, surface area of both samples ~ 50 m²/g).

S1.2. Physical chemical characterization

UV-Vis spectra of 0.1 M aqueous LA were recorded at room temperature in 1 mm quartz cuvettes using a Shimadzu UV-2401 PC spectrometer. The spectra were corrected for the adsorption of the solvent.

Photoelectrochemical properties of Pt/TiO₂, Pd/TiO₂ and Au/TiO₂ were examined with a controlled intensity modulated photospectroscopy setup (CIMPS by ZAHNER-elektrik, Germany) in a three-electrode cell configuration (Ag/AgCl and Pt as the reference and counter electrodes, respectively). 0.1 M LA solution was used as the electrolyte. Samples were illuminated with an UV LED ($\lambda = 385\text{nm}$) source. The photoelectrodes (working electrodes) were prepared by electrophoretic deposition of thin films of Pt/TiO₂, Pd/TiO₂ or Au/TiO₂ on FTO. The electrophoretic deposition was performed in a mixture of acetone (50 mL), the sample (100 mg) and iodine (30 mg). The FTO substrate, which acted as the cathode, was immersed in this mixture facing a Pt anode. Electrophoresis was carried out under a 20 V bias for 2 min. The obtained electrode was then dried under ambient conditions and calcined in air at 400°C for 2 h.

Fourier transform infrared spectroscopy (FTIR) measurements were carried out using a Bruker Vertex 70v instrument. FTIR spectra were recorded by averaging 32 scans in the range of 4000-400 cm⁻¹ at 2 cm⁻¹ resolution with a liquid nitrogen-cooled MCT detector. The samples were prepared as thin self-supporting wafers of 5-10 mg/cm² and placed inside a controlled environment infrared transmission cell,

capable of heating, cooling, gas dosing and evacuation. Prior to the measurements, all catalysts were evacuated at room temperature for 1 h and subjected to an additional thermal treatment at 100 °C for 1 h.

S1.3. Photolysis and photocatalysis activity tests

For the direct photolysis experiments a calculated amount of (LA) (90%, Sigma Aldrich) was added into deionized water to obtain solutions with LA concentrations of 0.02 M, 0.05 M, 0.10 M or 0.50 M. The pH of the 0.1 M lactic acid aqueous solution was 2.2. This value was then adjusted with HCl or NH₃·H₂O to obtain solutions of pH 1.0, 5.1 or 8.1.

Direct photolysis and photocatalytic decarboxylation of LA solutions were performed in a gas-tight system with a double-walled glass reactor (top-irradiated) equipped with a quartz optical window. For direct photolysis of LA at different pH, 80 mL of the 0.1 M LA with no catalyst was evacuated under stirring prior to irradiation to remove dissolved air. For direct photolysis of LA at different initial concentrations, 50 mL of the 0.1 M LA was evacuated under stirring prior to irradiation to remove dissolved air. For photocatalytic decarboxylation, 50 mL of 0.1 M LA solution with 50 mg TM/TiO₂ was treated under the same condition. The temperature of the reaction mixture was maintained at 20°C by cooling water. Reactions were carried out by irradiation with a 500W Hg (Xe) arc lamp (Oriental Instruments, Newport) equipped with a back-reflector. The IR part of the emission spectrum of the lamp was filtered out with a water filter. The reaction time was 3 h.

Gaseous products (i.e., H₂, CO, CO₂) were collected in the headspace of a gas-closed system and analysed in the course of the reaction with an online gas chromatograph (GC610 series, ATI UNICAM) equipped with a ShinCarbon column. The amount of H₂ produced was measured using a thermal conductivity detector with N₂ as the carrier gas; CO and CO₂ were detected using a flame ionization detector after conversion into CH₄ in a methanizer.

Qualitative analysis of the liquid products was performed by NMR (Varian 400 MHz spectrometer). All samples were prepared in a total volume of 0.5 mL in 5 mm NMR tubes, using 0.3 mL of DMSO as the internal standard. To identify the main products of the photolysis and photocatalytic decarboxylation of LA, high-resolution 2D HSQC NMR was performed using WET suppression of the H₂O resonance². Representative spectra for the direct LA photolysis and photocatalytic conversion with Pt/TiO₂ are shown in Figure S6.

Quantitative analysis of the liquid products was carried out by a combination of HPLC and GC-FID. An amount of 50 µl 1-propanol was added to the 50 mL reaction solution after each experiment and used as

the internal standard. Concentrations of LA and formic acid were analysed using a Shimatzu HPLC setup with 25 mM phosphate buffer of pH = 2 as mobile phase using a Prevail Organic Acid column. Acetaldehyde, ethanol, ethyl lactate, acetic acid, propionic acid and 2, 3-butanediol were quantified by GC-FID (Thermo GC equipped with a Stabilwax-DA column, 30 m × 0.53 mm × 1.0 μm). For both HPLC and GC-FID, the amount of products were determined using calibration curves generated with authentic compound solutions. Standards for all liquid products were obtained from Sigma-Aldrich.

The decarboxylation yield (Y) was calculated as follows:

$$Y (\%) = \frac{\mu\text{mol of product } CO_2 \text{ and } HCOOH \text{ formed}}{\mu\text{mol of lactic acid in the feed}} \times 100$$

or

$$Y (\%) = \frac{\mu\text{mol of product } CH_3CH_2OH, CH_3CHO \text{ and } 2 \times 2,3 - \text{Butanediol formed}}{\mu\text{mol of lactic acid in the feed}} \times 100$$

S1.4. Periodic DFT calculations

Periodic density functional theory (DFT) calculations were carried out using the Vienna Ab Initio Simulation Package (VASP)³ with the generalized gradient approximation (GGA-PBE)⁴. A plane-wave basis set with a cut off energy of 400 eV was used. Brillouin zone integration was carried out with single *k*-point (Gamma point) sampling. The convergence criteria for the force and energy are 50 meV/Å and 0.1 meV, respectively. For the simulations of the interface between Pt nanoparticle and TiO₂ surface, a slab model containing Pt₁₀ cluster⁵ and three O-Ti-O layers (5×2) TiO₂(110) was used with a vacuum space of 20 Å to avoid spurious inter-slab interactions. During geometry optimizations, the bottom layer was frozen, while the upper two layers were fully relaxed. All adsorbates were fully relaxed during geometry optimization. The DFT+*U* methodology⁶ (*U* is a Hubbard-like term describing the on-site Coulomb interactions) was used. *U*_{eff} was set to 4.0 eV⁷ to localize the electrons in the Ti 3d orbital. Dipole-moment corrections in the framework of periodic boundary conditions⁸ were employed to compensate for the non-symmetric configuration of the slab models. The udged elastic band algorithm⁸ was used to explore the minimum energy pathways and locate transition states. Frequency analysis confirmed that there was only one imaginary frequency along reaction coordinate for the transition states. For the transtion state for C-C cleavage, we carried out the frequency analysis by only relaxing the involved atoms and freezing the other atoms based on the optimized transtion state structure.

S1.5. Time-dependent DFT calculations

All DFT calculations were carried using the hybrid B3LYP⁹ exchange-correlation functional as implemented in Gaussian 09 D.01 program¹⁰. The all-electron 6-311+G(d,p) basis set was used for all atoms. The polarized continuum model (PCM) with standard parameters for water solvent was used to account for bulk solvent effects during geometry optimization, frequency analysis and excited state calculations. The excited state calculations and the simulation of UV-Vis spectra were carried out within the time-dependent DFT formalism¹¹. Previous studies confirmed the good accuracy of this methodology for the description of excited-state reactivity and photoexcitation processes of TiO₂ cluster models¹²⁻¹⁴.

The activation barrier for the direct non-catalytic photodecarboxylation of LA and lactate anions (Figure S5) were estimated from the relaxed potential energy scans carried out for the molecular species in the ground S0 and first excited S1 states.

Photoexcitation of the TiO₂-bound surface lactate species was carried out using the cluster model approach at the same level of theory as the other simulations. The initial configuration of the lactate complex and the cluster model representing the TiO₂ surface was constructed from the optimized periodic structure of the respective periodic slab model. To minimize potential artefacts due to the limited size of the cluster, the highly symmetric tricubic cluster model was used, in which all three Ti centers are in octahedral coordination after LA adsorption. The coordination environment of the Ti centers was completed by water molecules, resulting in a (TiO₂)₃·(H₂O)₆ cluster.

S2. Supplementary computational and experimental results

S2.1. Photolysis of aqueous lactic acid

Figure S1 summarizes the results of direct LA photolysis tests with varied pH of the solution. The highest reaction rate is observed at the unadjusted pH of 2.2 of the 0.1 M aqueous LA. The decreased reaction rate at lower pH is likely due to strong absorption of Cl⁻ anions in the UV region ($\lambda < 260$ nm) decreasing the quantum efficiency. The deprotonation of LA at higher pH and the concomitant decrease of the reaction rate points to lower reactivity of lactate anions, which is confirmed by TD-DFT calculations presented below in section 2.2.

Figure S2 shows UV-Vis spectra of 0.1 M aqueous LA in a 1.0 mm quartz cuvette, evidencing a strong absorption band below 250 nm. Excitation of the charge-transfer band ($\lambda \leq 254$ nm) leads to LA photodissociation and the initiation of the radical conversion path discussed in the main text.

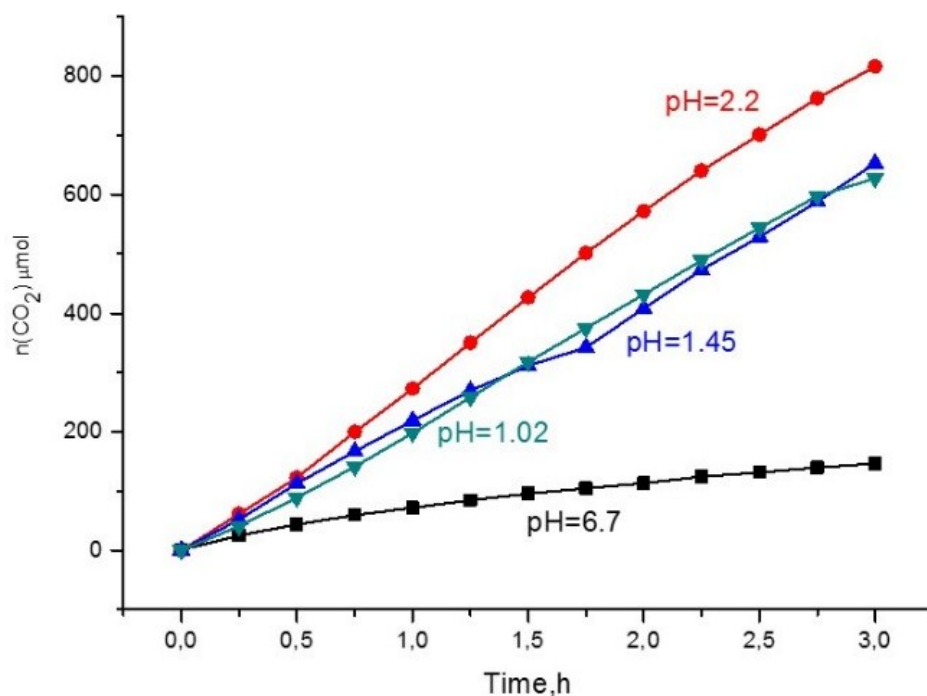


Figure S1. CO₂ evolution during irradiation of 0.1 M LA solution at varying pH (conditions: full output Hg(Xe) lamp, 500W; pH of 0.1 M LA solution without additives is 2.2; pH 1.45 and pH 1.02 LA solution were adjusted by HCl; pH 6.7 LA solution was adjusted by NH₃·H₂O).

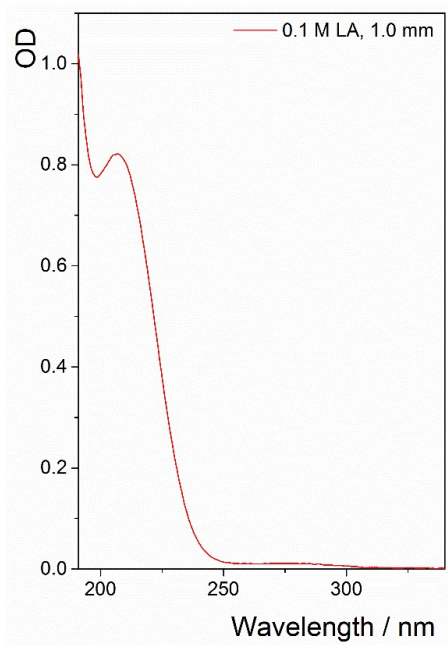


Figure S2. UV-Vis spectrum of 0.1 M aqueous LA.

S2.2. Time-dependent DFT calculations

Further insights into the mechanism of LA photoexcitation and photolysis were provided by TD-DFT calculations, whose results for both LA and lactate anion are summarized below in Tables S1 and S2, respectively. Molecular orbitals involved in the computed excitations are visualized in Figures S3 and S4, respectively.

Table S1. Results of TD-DFT calculations on lactic acid (TD-B3LYP/6-311+G(d,p), PCM(H₂O)).

Excitation NN	Energy, eV (nm)	Oscillator strength, f	CI expansion (largest coefficients, > 0.19)
1	6.02(206)	0.001	23→25 (0.63659) 24→25 (-0.27334)
2	6.38 (194)	0.030	23→25 (0.27142) 24→25 (0.6503)
3	7.16(173)	0.009	24→26 (0.6611) 24→27 (0.2204)
4	7.51 (165)	0.060	23→26 (0.66928)
5	7.76(160)	0.009	24→26 (-0.24089) 24→27 (0.61957)
6	8.03 (154)	0.007	21→25 (0.68064)
7	8.08(154)	0.022	22→25 (-0.3506) 23→27 (0.43651) 24→28 (-0.27836) 24→29 (0.26765)
8	8.10 (153)	0.044	22→25 (-0.20427) 23→27 (0.28012) 24→28 (0.56374)
9	8.14(152)	0.064	24→28 (0.22316) 24→29 (0.62858)
10	8.47(146)	0.015	22→25 (0.22843) 22→26 (0.61603) 23→27 (0.21313)

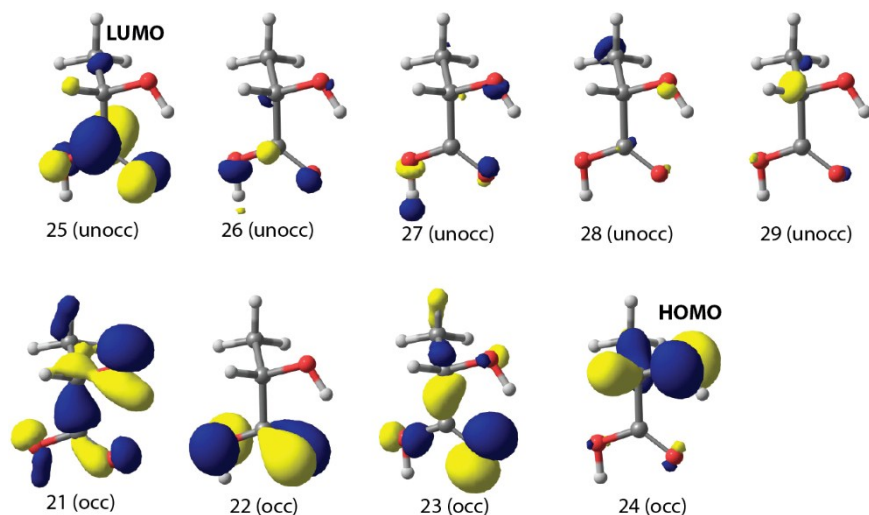


Figure S3. Frontier orbitals of LA involved in electronic excitations summarized in Table S1.

Table S2. Results of TD-DFT calculations on a lactate anion ($\text{CH}_3\text{CH}(\text{OH})\text{COO}^-$, LA^- , TD-B3LYP/6-311+G(d,p), PCM(H_2O)).

NN	Energy, eV (nm)	Oscillator strength, f	CI expansion (largest coefficients, $> 0.19 $)
1	5.72 (217)	0.009	24 → 25(0.6221) 24→29(0.25003)
2	6.04 (205)	0.018	24→25(-0.29027) 24 → 26(0.45183) 24→29(0.37135)
3	6.12 (203)	0.004	23 → 25(0.63736) 23→29(0.24688)
4	6.33 (196)	0.004	22 → 25(0.67857)
5	6.40 (194)	0.040	23→25(-0.23233) 23 → 26(0.51189) 23→27(-0.22875) 23→29(0.33429)
6	6.62 (187)	0.020	24→26(0.40293) 24 → 27(0.51805)
7	6.68 (186)	0.040	24 → 28(0.66946)
8	6.75 (184)	0.017	24→26(-0.21605) 24→27(0.38832) 24 → 29(0.45839)
9	6.79 (183)	0.017	21 → 25(0.61972)
10	7.01 (177)	0.023	22→26(0.28029) 23→26(0.38445) 23→27(0.34201) 23→29(-0.25042)

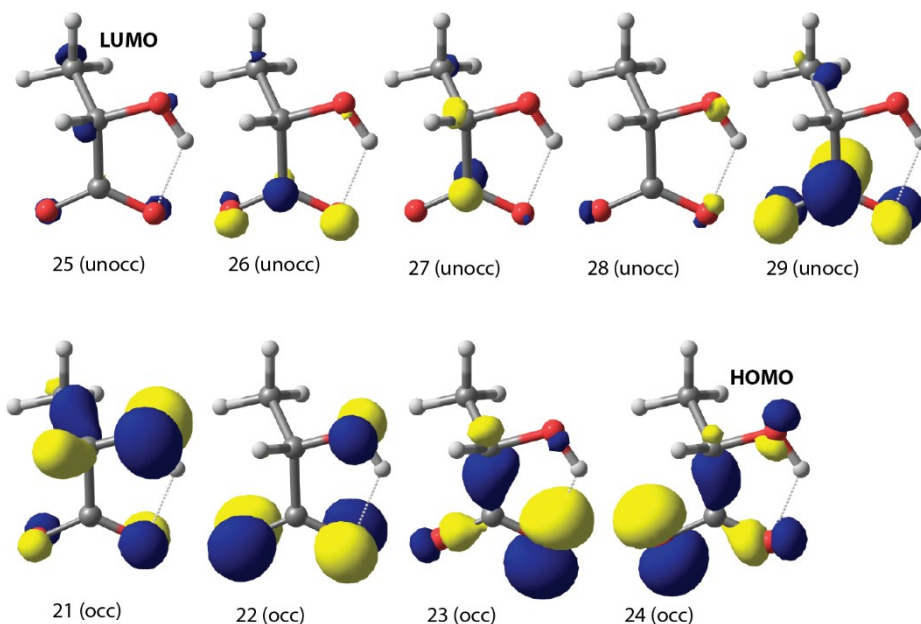


Figure S4. Frontier orbitals of LA⁻ involved in electronic excitations summarized in Table S1.

We further investigated the C-C bond cleavage process in both LA and lactate anion in the ground (S_0) and first singlet excited (S_1) states by scanning the potential energy surfaces along the C-C cleavage direction. The potential energy surface in S_0 state with respect to the C-C bond length were scanned (relaxed scans) with a step size of 0.02 Å for C-C bond lengths in the range of 1.48 Å to 2.50 Å. The results of these PES scans are shown in Figure S5a. The analysis of the decarboxylation path were carried out using TD-DFT. The respective potential energy surface relaxed scans in the S_1 state were performed with a step size of 0.1 Å by continuous elongating the C-C bond from 1.50 Å to 2.50 Å. The PES scans are shown in Figure S5b. In line with the experimental observations, photoexcitation is necessary to allow decarboxylation to occur. The overall barrier is lower for LA than for lactate. The estimated barrier for lactate decarboxylation is more than two times higher than for LA (Figure S5b).

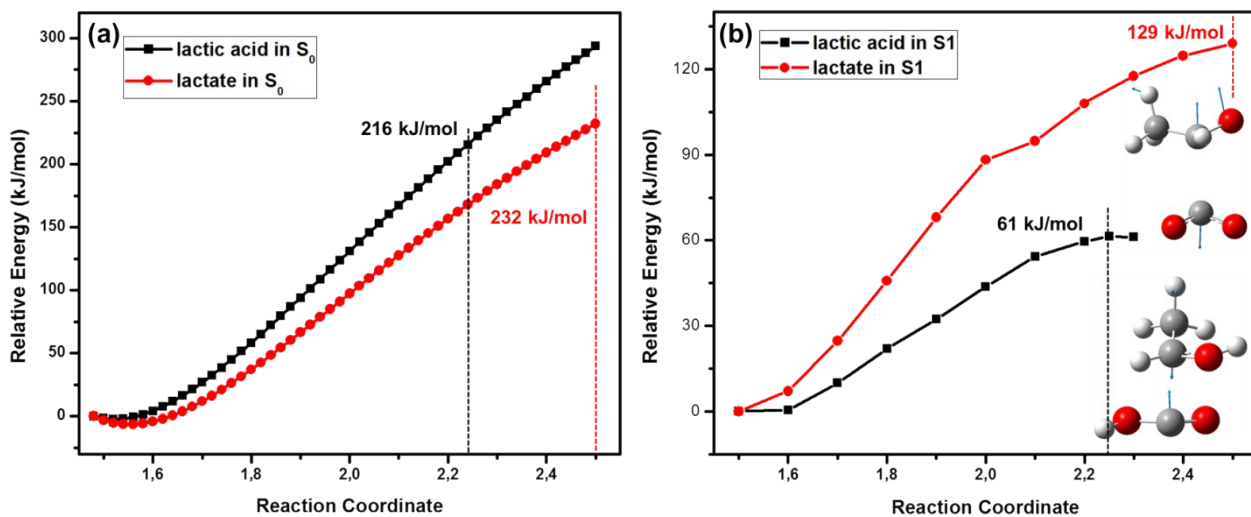


Figure S5. Relaxed PES scans (TD-B3LYP/6-311+G**) for LA and lactate anion in the ground S_0 (a) and first excited state S_1 (b) configurations in the water phase (PCM model, water as the solvent) based on time-dependent density functional theory calculations.

S2.3. Supplementary results of 2D NMR analysis and photoelectrochemical tests

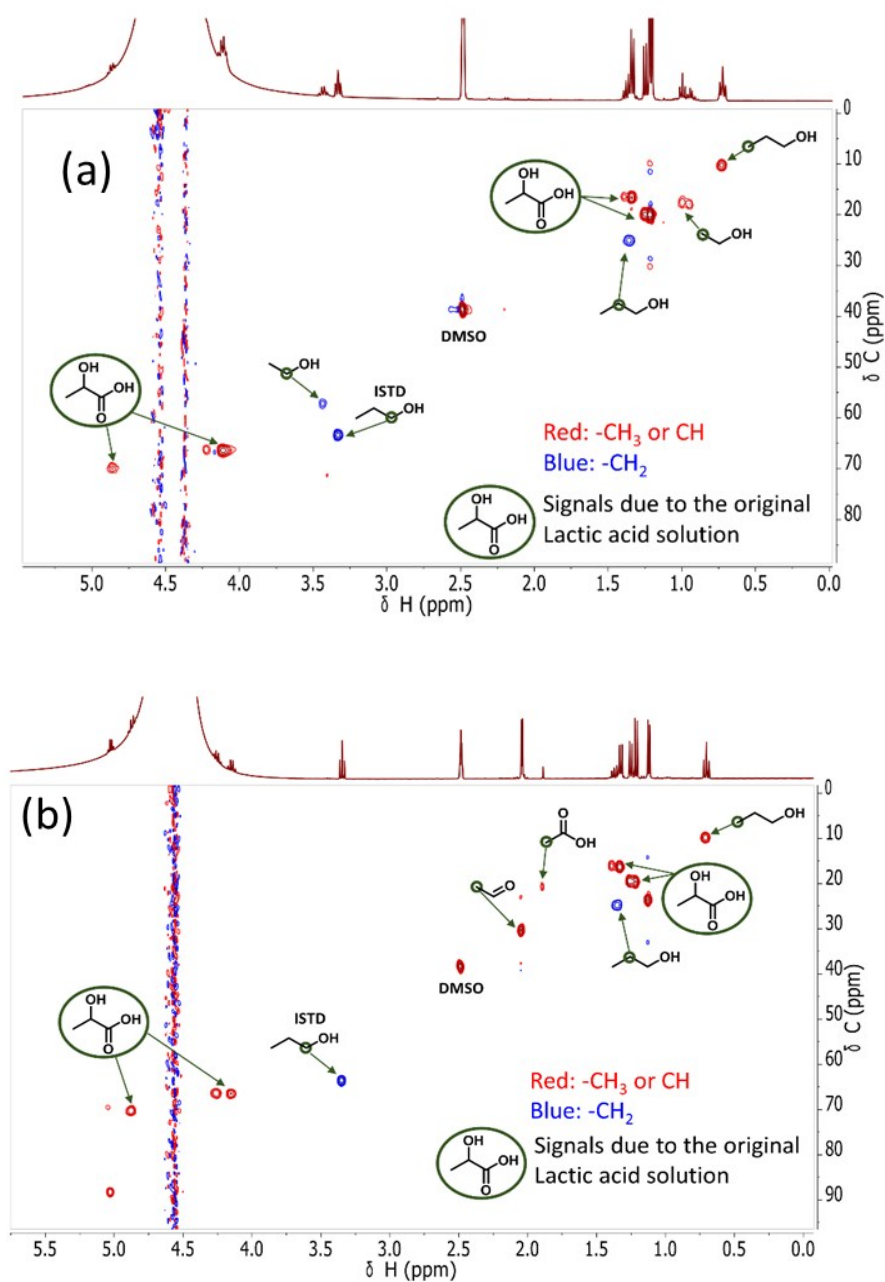


Figure S6. 2D HSQC NMR of reaction mixtures formed by LA (a) photolysis and (b) photocatalytic conversion in the presence of Pt/TiO₂ (Conditions: 50 mg catalyst, 50 mL 0.1 M LA aqueous solution, reaction time 3 h).

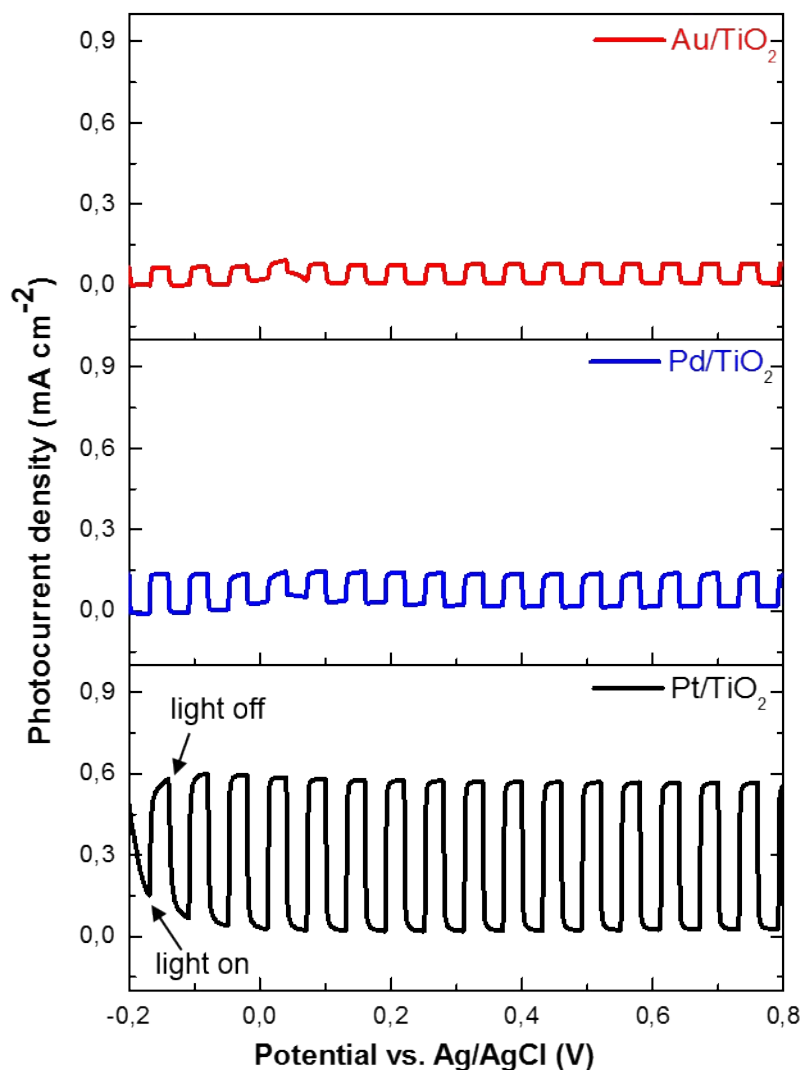


Figure S7. Photocurrent density versus applied potential (V versus Ag/AgCl) for Pt/TiO₂, Au/TiO₂ and Pd/TiO₂. A Pt wire was used as the counter electrode and Ag/AgCl served as a reference electrode. As the step $4 \rightarrow 1 + H_2$, **c** is shown in Figure 4, H₂ evolution is needed to close the catalytic cycle. Herein, Pt/TiO₂ shows the highest photocurrent, which correlates with the highest photodecarboxylation yield of LA (Table 1, entry 6).

S2.4. Photocatalytic conversion of ethanol and pyruvic acid

We carried out additional experiments using the best Pt/TiO₂ catalyst in an aqueous ethanol to elucidate whether the reaction mechanism of LA photodecarboxylation involves ethanol as an intermediate. Reaction conditions are shown in Table S3. In order to determine the possible role of pyruvic acid as an intermediate, we carried out an experiment using pyruvic acid as the substrate. The results are shown in Table S4. From where, we could find that Pt/TiO₂ did not increase the CO₂ amount comparing with the case without using photocatalyst. Besides Pt/TiO₂, we also tested LA photocatalytic conversions over Pt nanoparticulate catalysts supported on alumina, ceria under similar conditions (Table S5).

Table S3. Reaction Products of the photocatalytic reaction of ethanol

Catalyst	The amounts of products (μmol)					$X_{EtOH}(\%)$
	CH ₃ CHO	CH ₃ COOH	CO ₂	H ₂		
Pt/TiO ₂	642	41	0	650	19	

Reaction conditions: 50 mL 0.1 M ethanol aqueous solution; light source: Hg (Xe) lamp, 500 W, full output irradiation; reaction time: 3 h; catalyst loading: 50 mg 1 wt. % Pt/TiO₂.

Table S4. Reaction Products of the photocatalytic reaction of pyruvic acid

Substrate	Light source	Catalyst	The amounts of products (μmol)				X (%)
			CH ₃ CHO	CH ₃ COOH	CO ₂	H ₂	
LA	λ > 360nm	Pt/TiO ₂	801	10	715	985	49
Pyruvic Acid	Full output	No cat.	23	124	2409	0	83
Pyruvic Acid	Full output	Pt/TiO ₂	108	1019	2439	82	86

Reaction conditions: 50 mL 0.1 M aqueous solution; light source: Hg(Xe) lamp, 500 W; reaction time: 3 h.

Table S5. Reaction Products of the photocatalytic reaction of LA with other supports.

Substrate	Catalyst	The amounts of products (μmol)					X (%)
		CH ₃ CHO	EtOH	CH ₃ COOH	CO ₂	H ₂	
LA	Pt/ Al ₂ O ₃	18	30	0	0	0	0.3
LA	Pt/CeO ₂	13	0	0	0	0	0.2

Reaction conditions: 50 mL 0.1 M LA aqueous solution; light source: Hg (Xe) lamp, 500 W; Catalyst: 50 mg; reaction time: 3 h.

S2.5. Lactic acid adsorption on TiO₂ surface

The IR spectrum of LA adsorbed on bare TiO₂ and 1 wt. % Pt/TiO₂ are shown in Figure S8. $\nu(\text{OH})$ stretching bands are located in the range between 3740 and 3300 cm⁻¹. The sharp band observed at 3632 cm⁻¹ is attributable to hydroxyl group on TiO₂. LA readily interacts with this group, as can be derived from its erosion upon exposure to LA. The spectrum obtained after LA adsorption on TiO₂ shows new peaks at 1724 cm⁻¹, 1680 cm⁻¹, and 1568 cm⁻¹. The 1680 cm⁻¹ peak, red shifted by 44 cm⁻¹ relative to the similarly intense 1724 cm $\nu(\text{C}=\text{O})$ band, is likely due to the interaction of surface Lewis acid sites Ti⁴⁺ with the carbonyl oxygen atoms of LA on TiO₂. The relatively intense 1560 cm⁻¹ band stems from lactate. The band at 2991 cm⁻¹ is ascribed to $\nu_{\text{as}}(\text{CH}_3)$, the one 2941 cm⁻¹ to $\nu_{\text{s}}(\text{CH}_3)$, and the one at 2878 cm⁻¹ to $\nu(\text{CH})$.

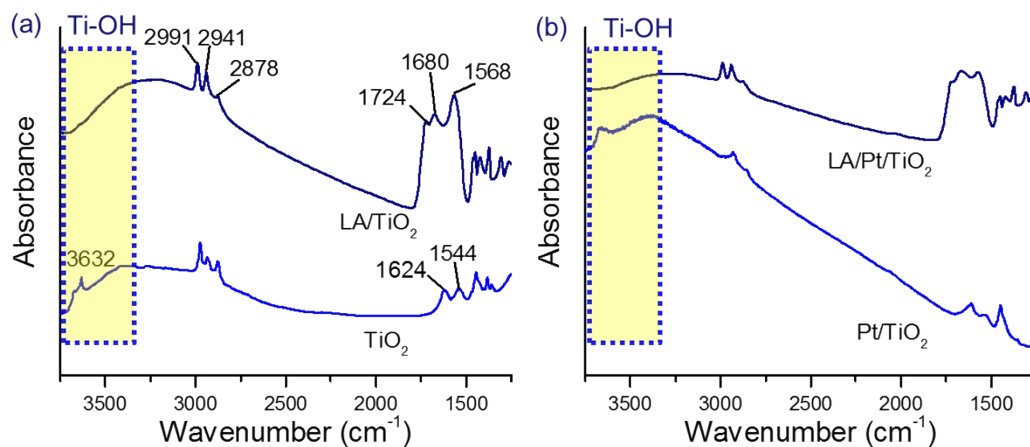


Figure S8. FTIR spectra of TiO₂ (a) and 1 wt. % Pt/TiO₂ (b) before (bottom) and after (top) exposure to LA vapor at room temperature. Changes in the OH-stretching region (yellow box) evidence a rapid reaction of LA with the surface hydroxyl groups, resulting in surface lactate species characterized by bands in the 1550-1750 cm⁻¹ region.

S2.6. Periodic DFT calculations on lactic acid decarboxylation over Pt10/TiO₂ model

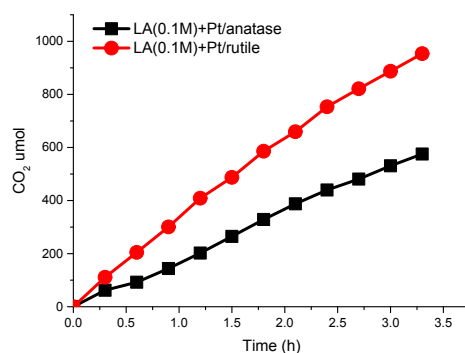


Figure S9. Comparison of LA photodecarboxylation for Pt on anatase and rutile forms of titania. Reaction conditions: 50 mL 0.1 M LA aqueous solution; 50mg Pt 1wt%/TiO₂; light source: Hg(Xe) lamp, 500 W.

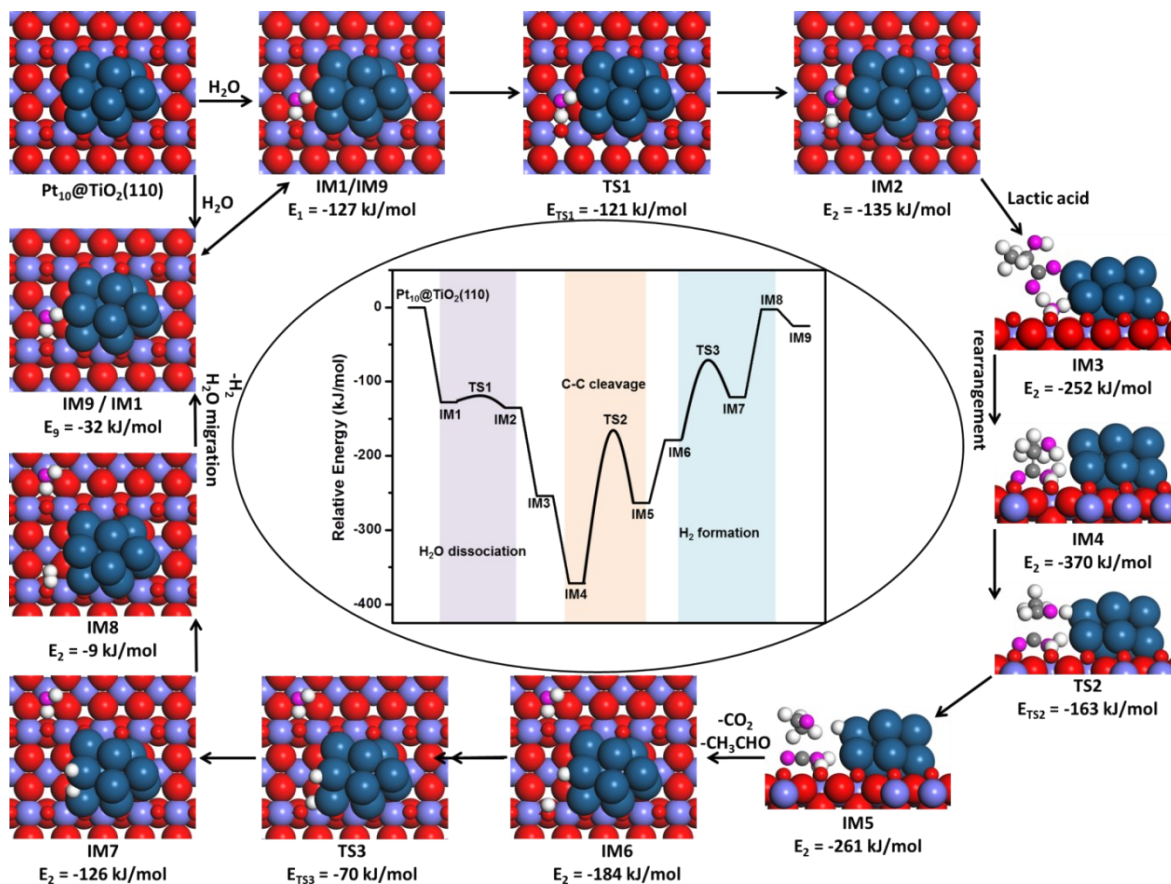


Figure S10. Mechanism of LA decarboxylation over Pt/TiO₂ constructed on the basis of the results of periodic DFT calculations. The numbers are relative energies (in kJ/mol) with a reference to free water, LA and a Pt₁₀@TiO₂ (110) model. Colour scheme for the atoms: pink – O of LA and water, red – O of TiO₂ (110), light blue – Ti, white – H, grey – C and dark blue - Pt.

Figure S10 summarizes the results of periodic DFT calculations for LA decarboxylation at the Pt₁₀@TiO₂ model. Water dissociation on the stoichiometric TiO₂ surface is very facile and results in basic and acidic surface hydroxyl groups; the barrier for this process is only 6 kJ/mol (IM1→ IM2). LA spontaneously reacts with the basic hydroxyl group to generate the lactate anion. The close proximity of the Pt cluster leads to interaction of Pt with the hydroxyl group of adsorbed lactate (IM3). Rearrangement of the adsorbates leads to a more stable state with the two carboxylic oxygen anions of LA coordinating to two Ti ions (IM4). In the ground state, the barrier for C-C cleavage is very high, i.e., 207 kJ/mol (IM4 → IM5). Herein, we argue that the C-C bond cleavage reaction to yield CO₂ and CH₃CHO is photo-assisted. At the same time, the H atom of the hydroxyl group is transferred to Pt. After CO₂ and CH₃CHO desorb, the acidic H atom bound to the titania surface bound hydroxyl group migrates to the Pt cluster with a barrier of 114 kJ/mol (IM6 → IM7). The final step is the recombination of the two H atoms to form molecular hydrogen (IM7 → IM8). The formation of H₂ in this way is similar to the photocatalytic reduction of water by Pt/TiO₂. The exact nature of the mechanism remains unclear, but it involves UV photon absorption.

S2.7. TD-DFT calculations on a TiO₂-bound surface lactate model

Table S6. Results of TD-DFT calculations on a lactate/TiO₂ cluster model (CH₃CH(OH)COO⁻/Ti₃O₁₂H₁₃⁺, TD-B3LYP/6-311+G(d,p), PCM(H₂O)).

NN	Energy, eV (nm)	Oscillator strength, f	CI expansion (largest coefficients, > 0.19)
1	4.245 (292)	0.001	111→112(0.61284) 111→113(0.24561)
2	4.291 (289)	0.003	111→112(-0.24583) 111→113(0.57978)
3	4.421 (280)	0.001	109→112(-0.24051) 109→113(-0.21606) 110→112(0.4115) 110→113(0.29578)
4	4.448 (279)	0.009	108→113(0.21881) 109→112(0.20865) 109→113(-0.19172) 110→112(-0.30951) 110→113(0.42704)
5	4.545 (273)	0.003	111→114(0.55258) 111→115(-0.22016)
6	4.598 (270)	0.001	108→113(-0.28177) 109→113(-0.33225) 109→115(-0.29511) 111→114(0.2265) 111→115(0.34377)
7	4.665 (266)	0.000	109→113(0.19997) 109→114(-0.238) 110→114(0.40446) 111→115(0.29352)
8	4.683 (265)	0.009	108→113(-0.22917) 109→113(-0.1994) 109→114(-0.20719) 110→114(0.34749) 111→114(-0.24367) 111→115(-0.23902)
9	4.753 (261)	0.050	108→113(-0.22917) 109→113(-0.1994) 109→114(-0.20719) 110→114(0.34749) 111→114(-0.24367) 111→115(-0.23902)
10	4.816 (257)	0.016	110→115(0.37014) 111→115(-0.25115) 111→116(-0.19607)

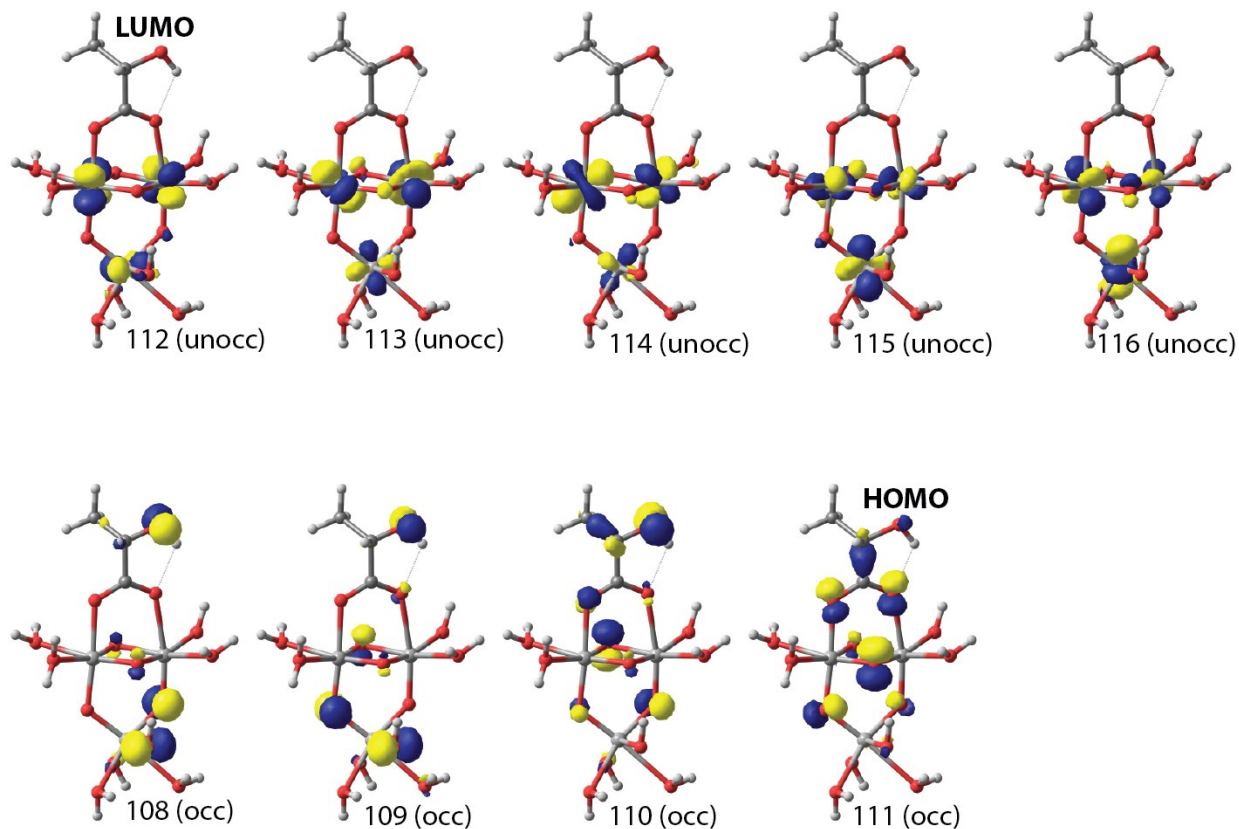


Figure S11. Frontier orbitals of LA involved in electronic excitations summarized in Table S4. The occupied orbitals 108-111 represent various linear combinations involving the MOs of the adsorbed lactate with some additional contributions due to the lone-pairs of the oxygen centers of the TiOx cluster. All the unoccupied orbitals 112-116 are linear combination of Ti 3d orbitals of the cluster.

S2.8. Acceptorless Dehydrogenative Coupling of lactic acid

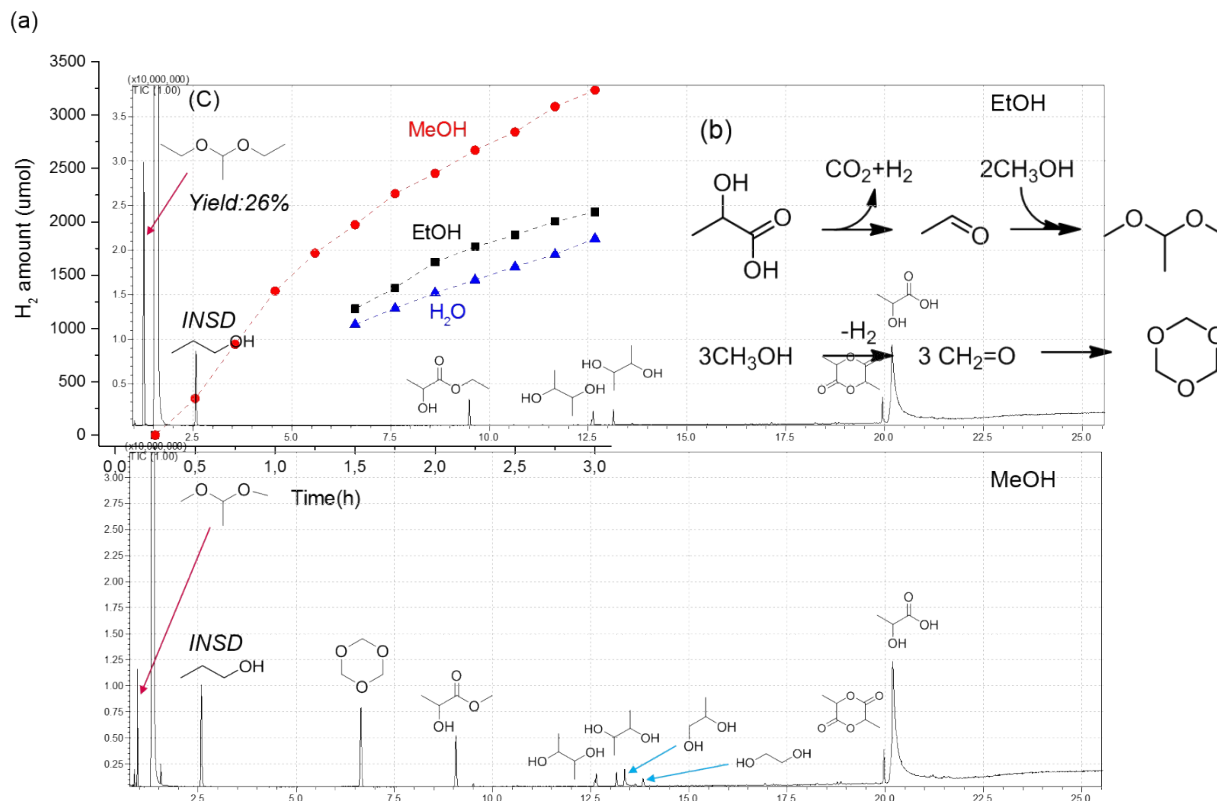


Figure S12. (a) Hydrogen evolution from LA solutions in ethanol, methanol and water: 50 mg Pt/TiO₂ in 50 mL 0.1 M LA aqueous solution under full output of the 500 W Hg (Xe) lamp. The increased hydrogen yield for the reaction in methanol can be explained by the mechanism (b) involving simultaneous LA dehydrogenative/decarboxylative coupling and methanol reforming. (c) GC-MS chromatograms of the reaction mixtures; the first peak before the solvent peak is an acetal which is formed by coupling decarboxylated LA to two solvent molecules. For ethanol, the yield of acetaldehyde diethyl acetal (ADEA) was 26% after 3 h reaction. For methanol, beside acetal also paraformaldehyde was formed.

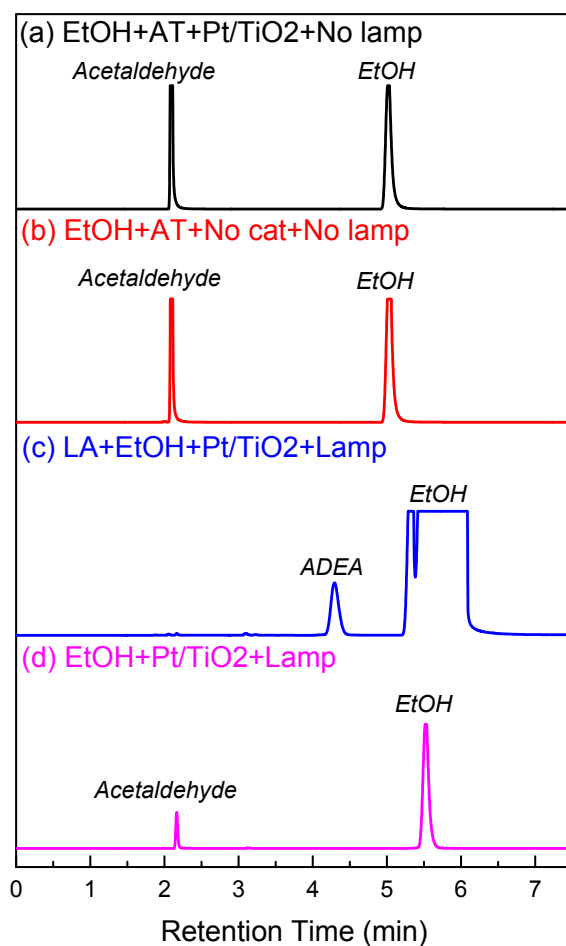


Figure S13. Gas chromatography of the liquid products from (a) mixture of ethanol and acetaldehyde without lamp irradiation by using Pt/TiO₂ as catalyst, stirring at RT for 3hs; (b) mixture of ethanol and acetaldehyde with neither lamp irradiation nor catalyst, stirring at RT for 3hs; (c) coupling experiment: LA in ethanol solvent, catalyst: Pt/TiO₂, light source: Hg (Xe) lamp, 500 W, full output irradiation; reaction time: 3 h; (d) Reaction: 50 mL 0.1 M ethanol aqueous solution; light source: Hg (Xe) lamp, 500 W, full output irradiation; reaction time: 3 h.

S3. References

- 1 Hugon, A., Delannoy, L. & Louis, C. Supported gold catalysts for selective hydrogenation of 1,3-butadiene in the presence of an excess of alkenes. *Gold Bulletin* **41**, 127-138
- 2 Griffith, E. C., Carpenter, B. K., Shoemaker, R. K. & Vaida, V. Photochemistry of aqueous pyruvic acid. *Proc. Natl. Acad. Sci. U.S.A.* **110**, 11714-11719 (2013).
- 3 Kresse, G. & Furthmüller, J. Efficiency of ab-initio total energy calculations for metals and semiconductors using a plane-wave basis set. *Comput. Mater. Sci.* **6**, 15-50 (1996).
- 4 Perdew, J. P., Burke, K. & Ernzerhof, M. Generalized Gradient Approximation Made Simple. *Phys. Rev. Lett.* **77**, 3865-3868 (1996).
- 5 Nelson, R. C. *et al.* Experimental And Theoretical Insights Into The Hydrogen-Efficient Direct Hydrodeoxygenation Mechanism Of Phenol Over Ru/TiO₂. *ACS Catal.* **5**, 6509-6523 (2015).
- 6 Dudarev, S., Botton, G., Savrasov, S., Humphreys, C. & Sutton, A. Electron-energy-loss spectra and the structural stability of nickel oxide: An LSDA+ U study. *Phys. Rev. B* **57**, 1505-1509 (1998).
- 7 Morgan, B. J. & Watson, G. W. A DFT+U description of oxygen vacancies at the TiO₂ rutile (110) surface. *Surf. Sci.* **601**, 5034-5041 (2007).
- 8 Sheppard, D., Terrell, R. & Henkelman, G. Optimization methods for finding minimum energy paths. *J. Chem. Phys.* **128**, 134106 (2008).
- 9 Becke, A. D. Density-functional thermochemistry. III. The role of exact exchange. *J. Chem. Phys.* **98**, 5648-5652 (1993).
- 10 Frisch, M. J., Trucks, G. W., Schlegel, H. B., Scuseria, G. E., Robb, M. A. C., J. R., Scalmani, G., Barone, V., Mennucci, B., Petersson, G. A., Nakatsuji, H., Caricato, M., Li, X., Hratchian, H. P., Izmaylov, A. F., Bloino, J., Zheng, G., Sonnenberg, J. L., Hada, M., Ehara, M., Toyota, K., Fukuda, R., Hasegawa, J., Ishida, M., Nakajima, T., Honda, Y., Kitao, O., Nakai, H., Vreven, T., Montgomery, J. A., Jr., Peralta, J. E., Ogliaro, F., Bearpark, M., Heyd, J. J., Brothers, E., Kudin, K. N., Staroverov, V. N., Kobayashi, R., Normand, J., Raghavachari, K., Rendell, A., Burant, J. C., Iyengar, S. S., Tomasi, J., Cossi, M., Rega, N., Millam, N. J., Klene, M., Knox, J. E., Cross, J. B., Bakken, V., Adamo, C., Jaramillo, J., Gomperts, R., Stratmann, R. E., Yazyev, O., Austin, A. J., Cammi, R., Pomelli, C., Ochterski, J. W., Martin, R. L., Morokuma, K., Zakrzewski, V. G., Voth, G. A., Salvador, P., Dannenberg, J. J., Dapprich, S., Daniels, A. D., Farkas, Ö., Foresman, J. B., Ortiz, J. V., Cioslowski, J. & Fox, D. J. *Gaussian 09, Revision D.01*, Gaussian, Inc.: Wallingford CT, 2009.
- 11 Stratmann, R. E., Scuseria, G. E. & Frisch, M. J. An efficient implementation of time-dependent density-functional theory for the calculation of excitation energies of large molecules. *J. Chem. Phys.* **109**, 8218-8224, (1998).
- 12 Berardo, E. *et al.* Modeling Excited States in TiO₂ Nanoparticles: On the Accuracy of a TD-DFT Based Description. *J. Chem. Theory Comput.* **10**, 1189-1199 (2014).
- 13 Sanchez-de-Armas, R., San-Miguel, M. A., Oviedo, J., Marquez, A. & Sanz, J. F. Electronic structure and optical spectra of catechol on TiO₂ nanoparticles from real time TD-DFT simulations. *Phys. Chem. Chem. Phys.* **13**, 1506-1514 (2011).
- 14 Chen, M., Straatsma, T. P. & Dixon, D. A. Molecular and Dissociative Adsorption of Water on (TiO₂)_n Clusters, n = 1–4. *J. Phys. Chem. A* **119**, 11406-11421 (2015).